Coupled-Single-Particle and Monte Carlo Model for Propylene Polymerization

Wei Wang, Zu-Wei Zheng, Zheng-Hong Luo

Department of Chemical and Biochemical Engineering, College of Chemistry and Chemical Engineering, Xiamen University, Xiamen, China 361005

Received 22 January 2010; accepted 12 April 2010
DOI 10.1002/app.32629
Published online 27 July 2010 in Wiley Online Library (wileyonlinelibrary.com).

ABSTRACT: A coupled-single-particle and Monte Carlo model was used to simulate propylene polymerization. To describe the effects of intraparticle transfer resistance on the polymerization kinetics, the polymeric multilayer model (PMLM) was applied. The reaction in each layer of the PMLM was described with the Monte Carlo method. The PMLM was solved together with the Monte Carlo model. Therefore, the model included the factors of the mass- and heat-transfer resistance as well as the stochastic collision nature of the polymerization catalyzed with single-site-type/multiple-site-type catalysts. The model presented results such as the polymerization dynamics, the physical diffusion effect, and the polymer molecular weight and its distribution. The simulation data were compared with the experimental/actual data and the simulation results from the uniform Monte Carlo model. The results showed that the model was more accurate and offered deeper insight into propylene polymerization within such a microscopic reaction–diffusion system. © 2010 Wiley Periodicals, Inc. J Appl Polym Sci 119: 352–362, 2011

Key words: computer modeling; kinetics (polym.); Monte Carlo simulation; poly(propylene) (PP); Ziegler–Natta polymerization

INTRODUCTION

In solid-catalyzed propylene polymerization, small catalyst particles (10–200 μm in diameter) are continuously fed into a reactor. The catalyst particles are composed of small fragments with a metal as the active center and are themselves porous. Propylene must diffuse through the boundary layer around the catalyst particles and through their pores to reach the active centers at which polymerization can take place.[1,2] Finally, the catalyst fragments grow into a broad distribution of polypropylene particles (1000–5000 μm in diameter).[1,2]

Up to now, many catalysts have been used in the polypropylene industry, and they can be divided into two types: single-site catalysts (normally silica-supported metallocene catalysts) and multiple-site catalysts (normally $MgCl_2$-supported Ziegler–Natta catalysts). The kinetics of solid-catalyzed polymerization is quite complex and may involve single or multiple sites on the catalyst surface. What is more complicated is that diffusion resistance may exist during the growth of the polymer particles.[1,2] However, the polymerization kinetics in the synthesis process is always an important part of polymerization engineering because of its key role in describing the relationship between the polymer properties and polymerization time.[1–4] Therefore, a number of models have been proposed to describe the kinetics of solid-catalyzed propylene polymerization.[2,5–22] In general, they are divided into two categories: physical models (single-particle models) and chemical models.

Physical models have been used to describe the interparticle and intraparticle mass and heat transfer during polymerization.[2,5–11] On the basis of the experimental evidence, it has been assumed that catalyst fragments in different radial positions are exposed to different concentrations of the monomer and chain-transfer agent (generally hydrogen) and consequently produce polymers with similar chain lengths but different spatial arrangements because of the diffusion resistance. Up to now, three single-particle models, namely, the solid-core model,[5] polymeric-flow model,[6,7] and multigrain model,[8] have been widely used to describe particle growth in the field of olefin polymerization. In addition, the polymeric multilayer model (PMLM), which is a versatile model, can also be used to simulate olefin polymerization.[11] From our point of view, some points linked to this work are as follows. First, the classical reaction–diffusion equation has been applied with the average chain propagation rate as the total polymerization rate in previous physical models. However, the actual polymerization rate at any time is

Correspondence to: Z.-H. Luo (luozh@xmu.edu.cn).
Contract grant sponsor: National Natural Science Foundation of China; contract grant number: 20406016.

the stochastic elementary reaction/collision rate. Second, the diffusion effect on the kinetics is increased because of the application of the classical reaction–diffusion equation. Finally, to the best of our knowledge, thus far, the application of the PMLM to solid-catalyzed propylene polymerization has not been common.

Models of the second category, chemical models,[4,12–22] neglect heat- and mass-transfer resistance in the polymer particle. In these models, in the case of single-site-type catalysts such as most metallocenes, a polymerization scheme can be used along with a set of kinetic constants. For multiple-site-type catalysts such as heterogeneous Ziegler–Natta catalysts, it has generally been assumed that two or more active site types are present, each one having a distinct set of constants for polymerization kinetics and therefore leading to different average properties of the polymer chains. The chemical models are mainly based on mathematical models. So far, some mainstream mathematical modeling techniques include the well-known method of moments,[23,24] the Galerkin *h–p* finite element method,[25,26] and continuous variable approximation.[27] The Galerkin *h–p* finite element method has been implemented in the commercial software package PREDICI, as developed by Wulkow.[28] The former two methods start with a population balance, and they both suffer from the enclosure problem when they are dealing with higher dimensionality. The continuous variable approximation method seems to be encountered more often for the modeling of random scission. Recently, the Monte Carlo method was introduced, and it has attracted more attention in the field of polymerization kinetics with the development of computer techniques and mathematical algorithms.[15–22,29] The Monte Carlo method is employed for problems when analytical or differential equation approaches are not feasible because of high dimensionality, especially in the case of very complex reaction schemes for which conventional methods require a high level of sophistication and include many simplified assumptions. The Monte Carlo method seems to be a simple and flexible alternative. Luo et al.[18] described the kinetics of propylene polymerization catalyzed with typical catalysts with a single-site/multiple-site (active) type in a liquid-phase stirred-tank reactor with the Monte Carlo method, but they ignored the mass- and heat-diffusion effects. Simon and Soares[30] developed a dynamic Monte Carlo model (MCM) to describe the chain length distribution of polyolefins produced with the help of coordination catalysts dependent on the polymerization time. They also ignored the physical diffusion. Simon et al.[31] also studied the copolymerization kinetics of ethylene and α-olefins by the Monte Carlo method. Although particular emphasis was given to the unique branch distribution of the copolymer, still the physical diffusion was ignored. Furthermore, Simon et al.[15] applied the Monte Carlo method to simulate the branching distribution in nickel diimine catalyzed polyethylene without considering the physical diffusion.

In practice, the effects of transfer resistances and catalyst site types on polymerization and product properties are evidently not exclusive; the heterogeneity caused by the presence of multiple-site types can be increased by transfer resistances during the polymerization. Both effects can affect the polymerization process and therefore the product properties because, for the diffusion–reaction system of propylene polymerization, models accounting for multiple-site types and transfer resistances simultaneously can provide the most complete description of the solid-catalyzed propylene polymerization.

In this work, we develop a comprehensive model for simulating the kinetics of solid-catalyzed propylene polymerization. To describe the effects of mass- and heat-transfer resistance on the kinetics, the PMLM is applied. The polymerization occurring in each layer of the PMLM is described by the Monte Carlo technique. The PMLM is solved together with the MCM. The comprehensive model, which combines the relative merits of the PMLM and Monte Carlo technique, is called the multilayer Monte Carlo model (MLMCM). In addition, the simulation data are compared with the experimental/actual data and the simulation results from the uniform MCM. The experimental/actual data have been collected from plants in which propylene polymerization follows the classical Himont Spheripol loop process by means of a continuously stirred tank (CSTR) in the presence of a fourth-generation Ziegler–Natta catalyst or silica-supported metallocene catalyst.[1]

MLMCM

Model idea

In our previous study,[18] we applied the Monte Carlo technique to simulate the kinetics of propylene polymerization. Our previous work distinguished the effects of single-site-type and multiple-site-type catalysts on propylene polymerization and product properties. In this work, our previous model is called the uniform MCM. Moreover, many experimental studies[32,33] have shown that a catalyst particle ruptures into many fragments (subparticles) during the initial stage of polymerization, and all the catalyst subparticles remain spherical during the polymerization. The monomer must diffuse through the boundary layer around the subparticles and through their pores to reach the active sites at which polymerization takes place. In essence, the catalyst is

TABLE I
Main Plant Parameters

Reactor type	Catalyst type	Polymerization process	Temperature (°C)	Time (h)
Continuous stirred-tank reactor (CSTR)	Fourth-generation Ziegler–Natta catalyst and metallocene catalyst (Himont catalysts)	Spheripol process (slurry system)	70	6

This table is based on refs. 1 and 34–36.

a microreactor and acts as a template during the growth of polymer particles, with one catalyst particle yielding one polymer particle. Therefore, it is possible to couple the MCM to the physical model.

Furthermore, as described previously, the later experimental/actual data have been collected from loop reactors in plants. The main plant operational parameters are listed in Table I. Under these conditions, it is possible to consider the loop reactors as CSTRs with a constant volume but with a variable reactor density.[1] In CSTRs, the mixed reactants (the monomer, active catalyst sites, etc.) can be considered to be uniformly distributed, and the heat transfer within and among the catalyst–polymer particles can be ignored.[1,2,8,9] In addition, for the fourth-generation Ziegler–Natta and silica-supported metallocene catalysts, their fragmentation and activation are instantaneous, and their initial sizes are adjacent. Therefore, for the coupled model, the following modeling assumptions have been made:[1,2,8,9,16]

1. Monomers and catalyst active sites within the reactor are uniformly mixed.
2. Catalyst particles are of the same size at the beginning of polymerization.
3. Heat transfer within and among the catalyst–polymer particles is negligible.
4. Catalyst particle fragmentation and activation take place instantaneously at time $t = 0$.

Moreover, the physical model applied in this work is the PMLM,[11] which accounts for the effect of diffusion resistance within the catalyst particle. For more information on the PMLM, the reader is encouraged to refer to Sun et al.[11] According to the PMLM, the catalyst–polymer particles are divided into many concentric, spherical layers, and microparticles are neglected.[11] Before polymerization, all layers have the same concentration of active sites as the whole catalyst particle. The bulk monomer diffuses with time from the edge of the particle into the inner layers and is driven by the monomer concentration gradient. The monomer diffusion between adjacent layers follows Fick's diffusion law. The Monte Carlo technique, which can reflect the stochastic collision nature during polymerization, is applied to simulate the reaction. Kinetic reactions occur when there are adequate monomer molecules and catalyst active centers within each layer. The radius of each layer should be recalculated with monomer concentration and polymerization rate data after a given time. On the basis of this model idea, it is obvious that the suggested model simulates the polymerization kinetics by coupling the PMLM and the Monte Carlo technique (i.e., the MLMCM). Furthermore, we emphasize here that the MLMCM concentrates on propylene homopolymerization microscale phenomena concerning different categories of single-site-type and multiple-site-type catalysts as well as the effects of diffusion resistance within the catalyst particle simultaneously.

The MLMCM is schematically shown in Figure 1. Detailed descriptions regarding the MLMCM are presented in the next sections.

Bulk kinetic scheme

The kinetic mechanism used in this work was introduced by Zacca et al.[1,34] Zacca et al. attributed the different natures of active site types to different oxidation states of the titanium atom, and they proposed for the Ziegler–Natta catalyst a two-site-type model reflecting the oxidation state of the catalyst from Ti^{3+} to Ti^{2+}. The two-site-type kinetic model can be presented as follows:

$$\text{Site activation:} \quad C^* \xrightarrow{k_a^k} P_0^k \tag{1}$$

$$\text{Initiation:} \quad P_0^k + M \xrightarrow{k_i^k} P_1^k \tag{2}$$

$$\text{Propagation:} \quad P_r^k + M \xrightarrow{k_p^k} P_{r+1}^k \tag{3}$$

$$\text{Site deactivation:} \quad P_r^k \xrightarrow{k_d} C_d + D_r^k \tag{4}$$

$$\text{Site transformation:} \quad P_r^k \xrightarrow{k_t} P_r^I \tag{5}$$

$$\text{Chain transfer:} \quad P_r^k + H_2 \xrightarrow{k_{tH}^k} P_0^k + D_r^k \tag{6}$$

where, H_2 is hydrogen; C* is the active site; D_r^k is the dead polymer of chain length r on the kth type of active site; k_a^k, k_1^k, k_p^k, k_d, k_t, and k_{tH}^k are the reaction rate constants on the kth type of active site; M is the monomer; and $P_r^{k(l)}$ is the living polymer chain of length r on the kth (lth) type of active site.

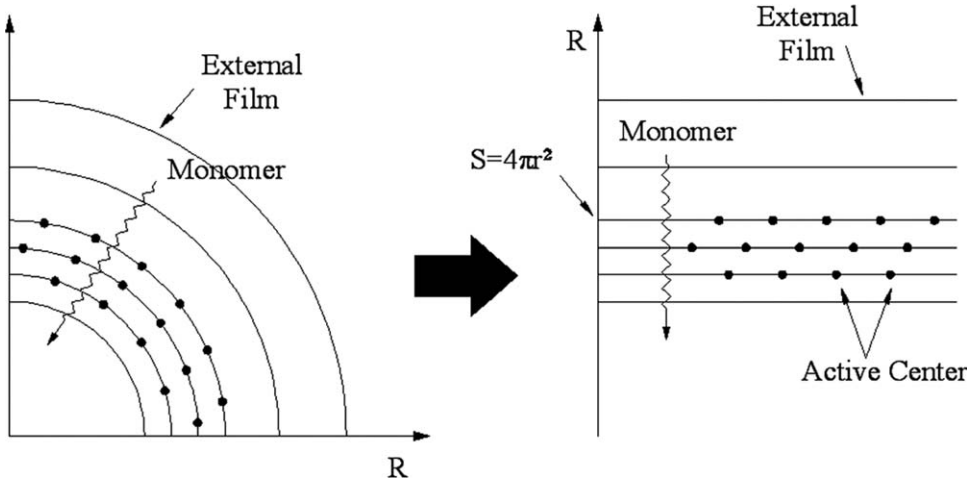

Figure 1 Equivalent interpretation of the MLMCM used in this study (R is the radius of each layer, and S is the area of each layer).

The bulk kinetic model eliminates the site transformation when it simulates propylene polymerization catalyzed with a single-site-type catalyst (silica-supported metallocene). In practice, the site transformation reaction reflects the uniform type of active center of the catalyst, which is the main distinction from the two-site-type kinetic model. The parameters used in these two kinetic models are shown in Tables II and III, respectively.

Model algorithm

The MLMCM has been derived and partially inherited from the PMLM for the sake of diffusion consideration. The Monte Carlo simulation can be described as follows.

The innermost layer is considered to be a solid core in which polymerization does not take place, and its volume remains unchanged during the polymerization. The outer part of the catalyst–polymer particle is divided into 10 concentric, spherical layers in which catalyst active centers are uniformly distributed. Monomer molecules diffuse through the bulk phase into different particle layers driven by the monomer concentration gradient. D_1 represents the diffusion coefficient between adjacent particle layers. ρ_{pol} and d_{pol} denote the density of the polymer and the initial particle diameter, respectively. Parameters for the diffusion effect are not treated separately for single-site-type and two-site-type MLMCMs; they are shown in Table IV and are based on refs. 8 and 35–37.

Monomer concentrations within each layer should be updated after a given interval. According to Fick's diffusion law, the number of monomer molecules transferred between adjacent layers because of the concentration gradient can be determined as follows:

$$\Delta M = D_1 \times (M_i - M_{i-1})/(R_i - R_{i-1}) \times 4\pi R_{\text{avg}}^2 \times \Delta t \times N_A \quad (7)$$

$$R_{\text{avg}} = (R_i + R_{i-1})/2 \quad (8)$$

where, N_A is the Avogadro's number; ΔM is the monomer concentration gradient between adjacent layers; M_i and M_{i-1} are the monomer concentrations of the ith and $(i - 1)$th layers, respectively; R_{avg} is the average radial position as described in eq. (8), R_i

TABLE II
Simulation Parameters Used for the Two-Site-Type Model ($TiCl_4/MgCl_2$ Ziegler–Natta Catalyst)

Parameter	Unit	Value at 70°C	Reference
[Al]	mol/m^3	10	8
χ_{Ti}^*	—	0.40	1,34
μ_1	—	0.8064	1,34
μ_2	—	0.1936	1,34
M_b	mol/m^3	9917	1,34
ϕ	—	0.479	1,34
k_p^1	$m^3/mol/s$	0.3428	1,34
k_p^2	$m^3/mol/s$	0.03428	1,34
k_i^{12}	s^{-1}	2.835×10^{-4}	1,34
k_d^2	s^{-1}	7.95×10^{-5}	1,34

TABLE III
Simulation Parameters Used for the Single-Site-Type Model (Metallocene Catalyst)

Parameter	Unit	Value at 70°C	Reference
[Al]	mol/m^3	10	14
χ_{Ti}^*	—	0.40	8,12
M_b	mol/m^3	9917	8,12
ϕ	—	0.479	8,12
k_p^1	$m^3/mol/s$	0.2691	8,12
k_d^1	s^{-1}	1.811×10^{-4}	8,12

TABLE IV
Diffusivity Parameters for the MLMCM

Parameter	Unit	Value	Reference
ρ_{pol}	kg/m^3	905	8
D_1	m^2/s	10^{-9}	35, 36
d_{pol}	m	10^{-7}	35, 37

and R_{i-1} are the radial positions of the ith and $(i-1)$th layers in the growing polymer particle, respectively; and Δt is a predetermined time interval determined according to the reaction time interval in the outermost layer. Therefore, Δt can be determined with the following equation:[19–21]

$$\Delta t = \tau = \frac{1}{\sum_{i=1}^{n} c_i h_i} \ln(1/r_3) \tag{9}$$

where, c_i is the stochastic rate constant, h_i is the number of reactant molecules of the ith elementary reaction, n is the overall number of elementary reactions, r_3 is a random number, and τ is the time interval.

The layers within catalyst–polymer particles are always growing when propagation occurs. After each reaction step, the radius and volume of each layer should be recalculated:

$$V_i^0 = \frac{4\pi}{3}\left[\left(r_{i+1}^0\right)^3 - \left(r_i^0\right)^3\right] \tag{10}$$

$$V_i^{k+1} = V_i^k\left[\frac{R_p MW \Delta t}{\rho_p} + 1\right] \tag{11}$$

$$r_{i+1}^{k+1} = \left[\frac{3}{4\pi} V_i^{k+1} + \left(r_i^{k+1}\right)^3\right]^{\frac{1}{3}} \tag{12}$$

where

$$R_p = k_p M_i P_{act}, \quad P_{act} = \sum_{j=1}^{\infty} P_j.$$

where, P_{act} and P_j are the total and the jth reaction probabilities, respectively; r_i is the radial radius of the ith layer; R_p is the polymerization rate; V_i^k is the volume of the ith layer on the kth type of active site; W is the monomer molecule mass; ρ_p is the particle density; Δt is the time interval.

A detailed flow chart of the MLMCM algorithm is given in Figure 2. The initial simulation conditions, including selected parameter data in the MCM,[18] were the same as those in the MLMCM.

The simulation of the single-site-type MLMCM was almost the same, except that it was compared to different site types in the two-site-type MLMCM.

RESULTS AND DISCUSSION

Polymer yield profile

Because the main parameters used in this model were selected from refs. 1, 8, 12, and 34, the results derived from our model were first quantitatively compared with the original ones. In addition, the simulation data of the model were compared with the simulation data of the MCM.

The polymerization kinetics at 70°C was simulated with the aforementioned MLMCM. A series of simulation results, including the polymer yield, polymer molecular weight and its distribution, fraction of active centers, and layer radius evolution, was obtained. Although the yield data could be directly obtained from polymerization experiments and were reported previously,[1,38] the data for the time dependence of the yield were used to verify the model.

Figures 3 and 4 present profiles of the polymer yields at different polymerization times versus the experimental data with the single-site-type and two-

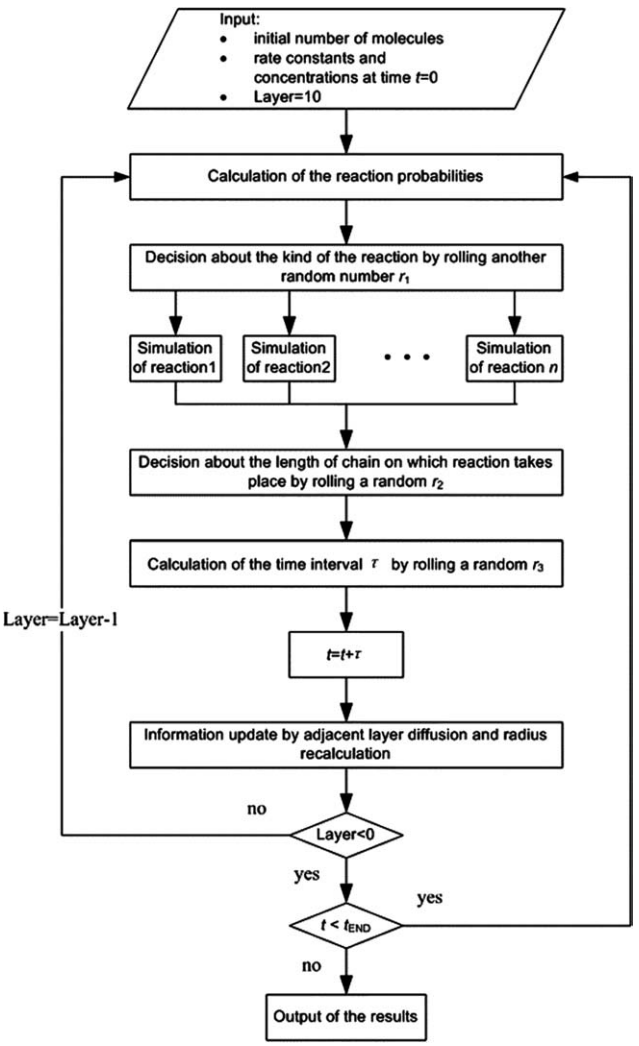

Figure 2 Flow sheet of the MLMCM methodology.

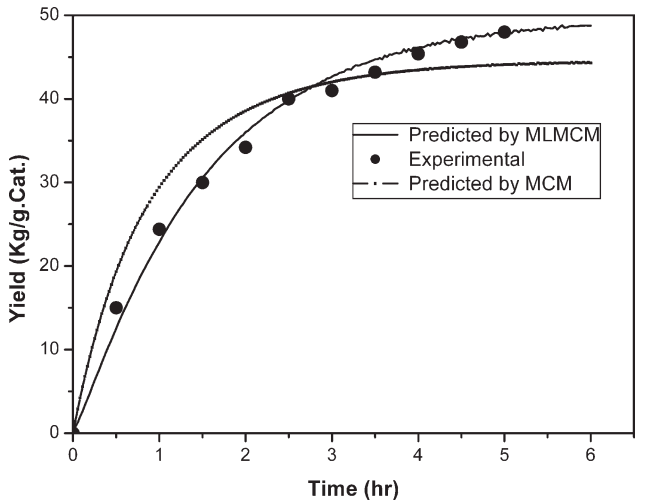

Figure 3 Polymerization yield versus the time with the single-site-type MLMCM and MCM.

site-type MLMCMs, respectively. The correlation coefficients between the predictions by the single-site-type and two-site-type MLMCMs and the experimental data of Di Drusco and Rinaldi[1,38] could be as high as 0.9990 and 0.9993, respectively. The correlation coefficients between the predictions by the single-site-type and two-site-type MCMs and the experimental data are 0.9923 and 0.9925, respectively. This shows that the predictions by the MLMCMs are more fitted to the experimental data obtained by Di Drusco and Rinaldi than those from the MCMs. This is because the MLMCMs provide a more precise description of propylene polymerization with a diffusion effect than the MCMs. Actually, the diffusion resistance restrains the rapid increase in the polymer yield at the initial stage of polymerization and increases the value of the yield at the end of polymerization.

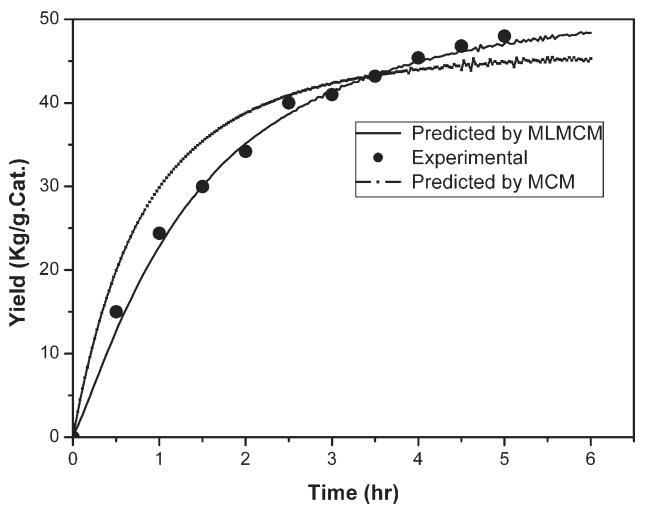

Figure 4 Polymerization yield versus the time with the two-site-type MLMCM and MCM.

According to the yield curves shown in Figures 3 and 4, the polymerization process can be divided into three temporal sections. The first section is diffusion-dominated. Because of the diffusion resistance, monomers around the catalyst active center are no more excessive, even it suffers from monomer starvation at the inner layers in this section. The MLMCM shows this kind of phenomenon, which is extremely obvious in the first hour of polymerization. In this section, the timescale of the reaction is negligible versus the timescale of diffusion, which is a slow and dominated process. Meanwhile, as time continues, the monomer concentration values within different layers become closer to one another, and this makes the driving force of Fick's diffusion lower. For 1–4 h, the state of monomer starvation no longer exists, and the monomer begins to accumulate around the catalyst active centers. This section should be called reaction-dominated because the reaction within each layer becomes the key factor during this time period. The last section is still steady-state because when the concentration of the monomer and active site goes down, there is no distinct increase in the yield curve any more.

Polymer number-average chain length profile

In this work, the number-average chain length data were also obtained and used to verify the model. Figures 5 and 6[39,40] present profiles of the number-average chain length at different polymerization times in contrast to the actual (experimental) data with the single-site-type and two-site-type MLMCMs, respectively. According to Figures 5 and 6, we can confirm that the number-average chain length data predicted by the MLMCMs were more

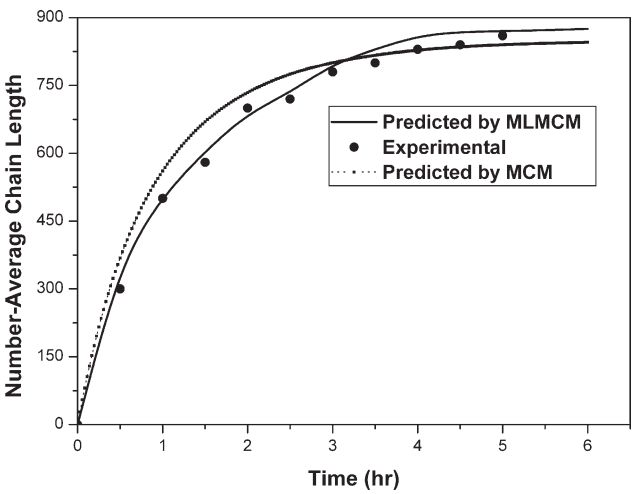

Figure 5 Polymer number-average chain length versus the time with the single-site-type MLMCM and MCM (the polymerization conditions were the same as those used for Figures 3 and 4 and reported in refs. 1 and 34).

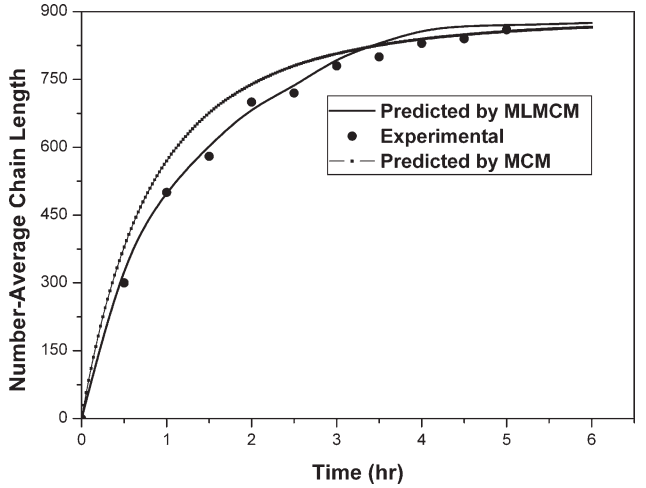

Figure 6 Polymer number-average chain length versus the time with the two-site-type MLMCM and MCM (the polymerization conditions were the same as those used for Figures 3 and 4 and reported in refs. 1 and 34).

fitted to the actual data than those from the MCMs. In practice, the aforementioned results derived from the MLMCMs provide a more precise description of propylene polymerization with a diffusion effect than the MCMs. In addition, the main parameters used in this work are connected to the yield data in refs. 1 and 38 and are still the parameters used to obtain the number-average chain length data by the MLMCMs (MCMs). Accordingly, the predicted precision shown in Figures 5 and 6 is less than that in Figures 3 and 4. However, in all, we can find that all correlation coefficients between the predictions by the single-site-type and two-site-type MLMCMs and the actual data could be up to 0.9000 according to Figures 5 and 6. Besides, Figures 5 and 6 show that the predicted curves by MCMs are more even than those by MLMCMs. They also show that the number-average chain length indicates an asymptotic

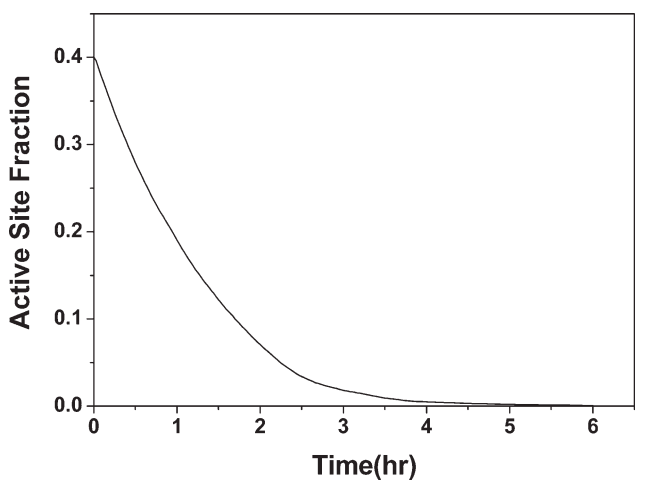

Figure 7 Fraction of active sites versus the time with the single-site-type MLMCM.

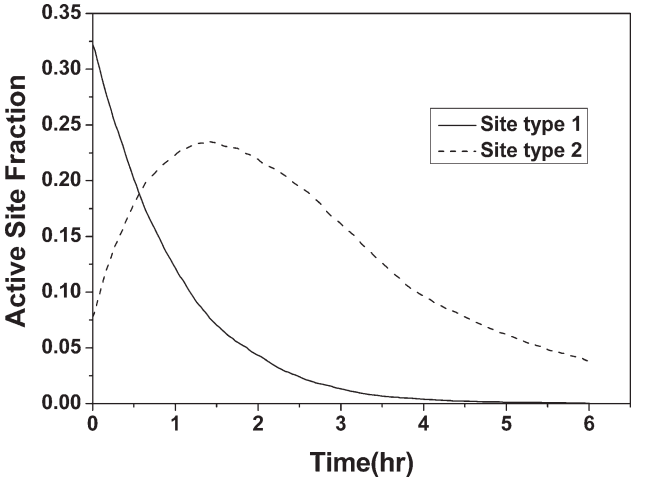

Figure 8 Fraction of active sites versus the time with the two-site-type MLMCM.

increase approaching their maximum values. For detailed descriptions of this change, readers are encouraged to refer to our past work.[18]

Active site fraction profile

The active site concentration transformation was investigated with the MLMCM. Because there is no transformation reaction in the single-site-type MLMCM, as shown in Figure 7, the concentration of the active centers drops with time on account of the deactivation reaction. Meanwhile, the multiple-site-type MLMCM assumes that the first site type (Ti^{3+}) transforms into a lower oxidation state (Ti^{2+}) over time that is less active with propylene. As shown in Figure 8, the assumption gives rise to the fact that the fraction of active site type 1 decreases rapidly to almost 0 after 4 h of polymerization, and this promotes the fraction of active site type 2 to a

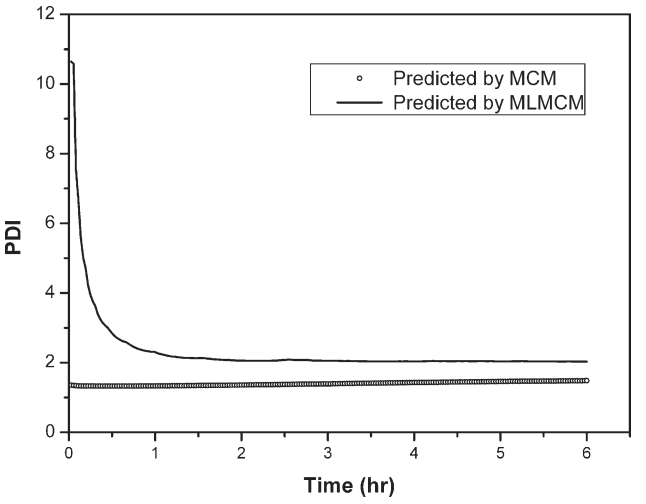

Figure 9 PDI versus the time with the single-site-type MLMCM and MCM.

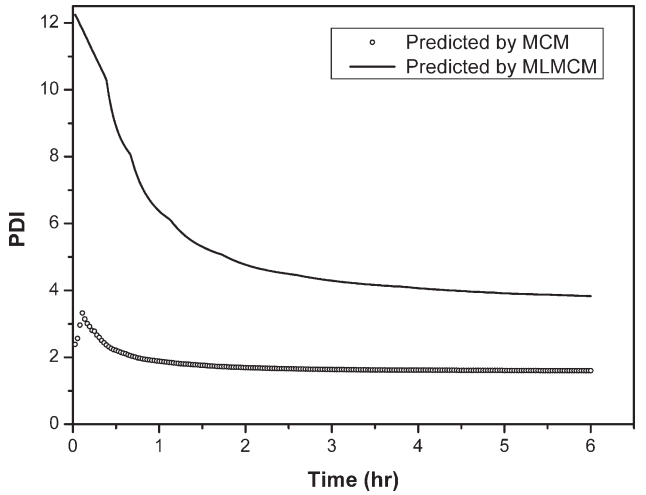

Figure 10 PDI versus the time with the two-site-type MLMCM and MCM.

maximum value of about 24% after 2 h of polymerization. The fraction of active site type 2 then declines to about 5% in the next 4 h of polymerization because of its deactivation reaction.

Polydispersity index (PDI) profile

Figures 9 and 10 show the evolution of PDI with the single-site-type and two-site-type MLMCMs and MCMs, respectively. The single-site-type MLMCM can predict a narrow molecular weight distribution with a PDI value of 2, which is precisely the theoretical value predicted by Flory.[41] The case is totally different for the two-site-type MLMCM: the PDI of the final polymer can be up to almost 4 (larger than the former one). In addition, according to Figures 9 and 10, we can know that the predicted PDIs for the final polymer by the single-site-type and two-site-type MCMs are about 1.8 and 2, respectively. On the whole, the nature of the catalyst multicenter makes

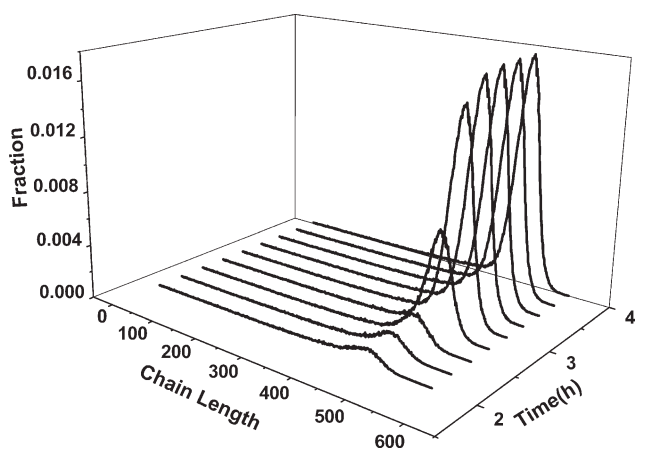

Figure 11 MCD evolution with the single-site-type MLMCM at intervals of 900 s.

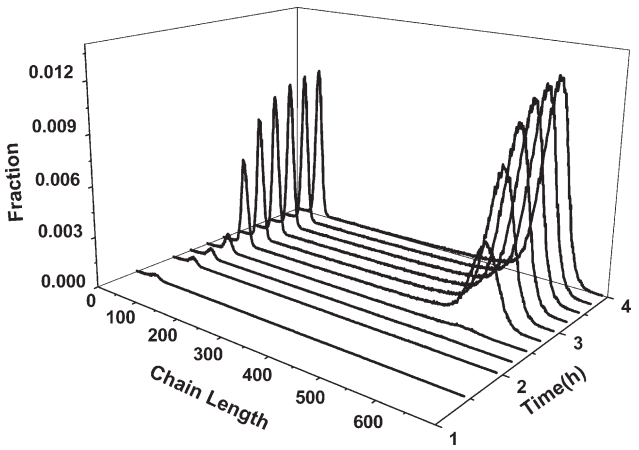

Figure 12 MCD evolution with the two-site-type MLMCM at intervals of 900 s.

contributions to a broader molecular weight distribution. Furthermore, the diffusion effect can make the polymer PDI much higher.[5–11] Therefore, the PDI data predicted by the single-site-type and two-site-type MCMs (MLMCMs) are different. Moreover, the PDI data predicted by the MLMCM are more fitted to the industrial and experimental PDI data than those from the MCM.[41] Accordingly, the MLMCM does have an advantage in precisely simulating propylene polymerization and predicting the product properties.

Polymer molecular chain length distribution (MCD) profile

The polymer molecular weight distribution was also obtained with the MLMCM. Here, the molecular weight distribution was based on the chain length (i.e., MCD).

The simulation data at intervals of 900 s are listed in this work and are shown in Figures 11 and 12; they clearly show corresponding messages. Here, Figures 11 and 12 show the MCD evolution with the

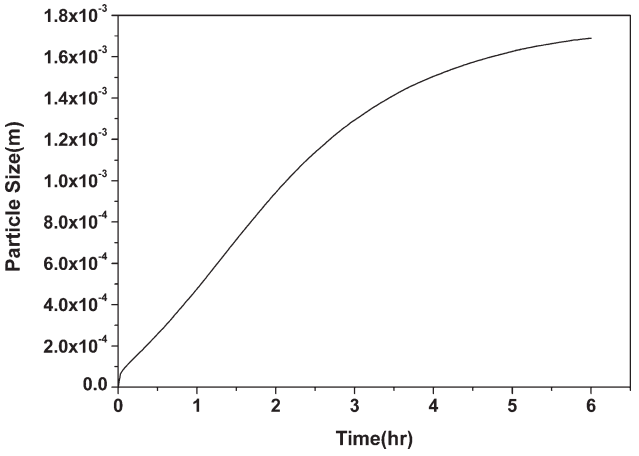

Figure 13 Particle size evolution with the single-site-type MLMCM.

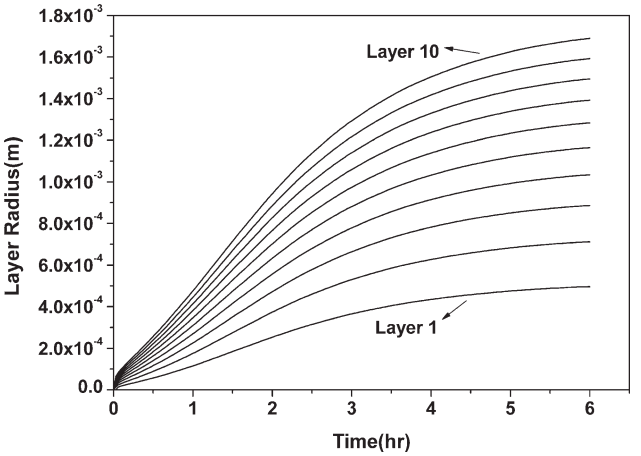

Figure 14 Layer radius evolution with the single-site-type MLMCM (the innermost layer in which polymerization did not take place was layer 0).

single-site-type and two-site-type MLMCMs at intervals of 900 s, respectively.

According to Figures 11 and 12, we can see that the active polymer MCD increases and the distribution property of the polymers also changes during the beginning of polymerization. The polymer MCD approaches a constant level as the polymerization proceeds and reaches a constant value after about 3.5 h. That is, the distribution property of the polymers is basically constant since 3.5 h. In practice, according to Figures 3 and 4, it is obvious that the low concentrations of the monomer and active chains correspond to the parallel line with the time coordinate. Accordingly, it leads to a small probability of chain propagation since 3.5 h. It also proves that the viewpoint of the steady-state section obtained from the MLMCMs is correct. Furthermore, according to Figure 11, the simulated MCD of the final polymers by the single-site-type MLMCM exhibits a single peak. However, the simulated MCD

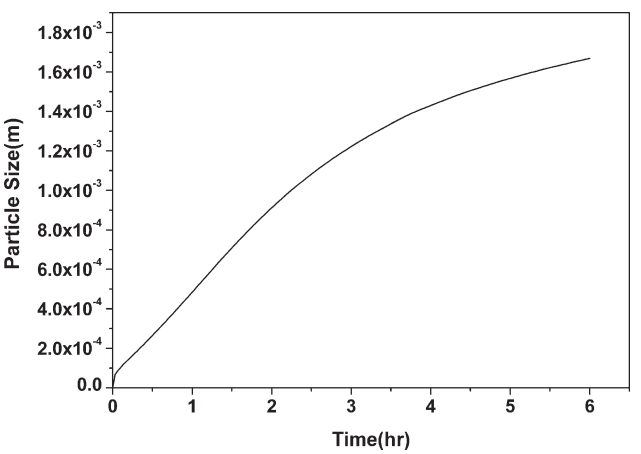

Figure 15 Particle size evolution with the two-site-type MLMCM.

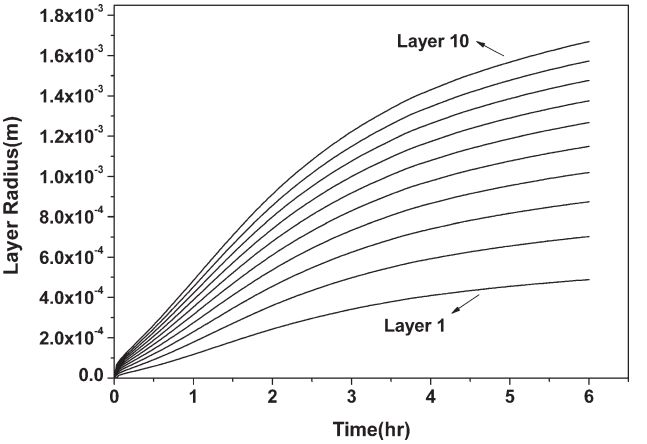

Figure 16 Layer radius evolution with the two-site-type MLMCM (the innermost layer in which polymerization did not take place was layer 0).

of the final polymers by the two-site-type MLMCM shows two peaks, as shown in Figure 12.

Particle size profile

On the other hand, the MLMCM is a discrete description of a propylene polymerization system. The reaction and diffusion are interrelated within the MLMCM because the reaction within each layer makes a contribution to the expansion of the layer radius, and meanwhile, the layer radius has a direct effect on the amount of the monomer between the adjacent layers. More combination research of these two factors could make much more sense for validating our model.

Derived from the single-site-type MLMCM, Figures 13 and 14 present the catalyst–polymer particle size evolution and layer radius evolution, respectively. In the diffusion-dominated period, the rate of increase in the particle layer is not so fast because

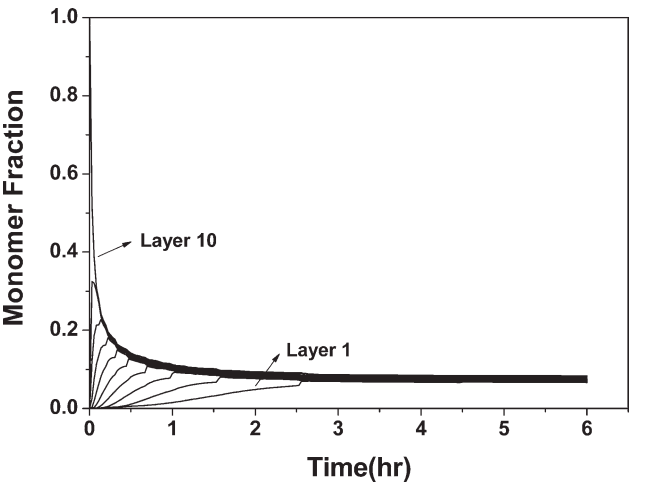

Figure 17 Monomer fraction evolution within each layer with the single-site-type MLMCM.

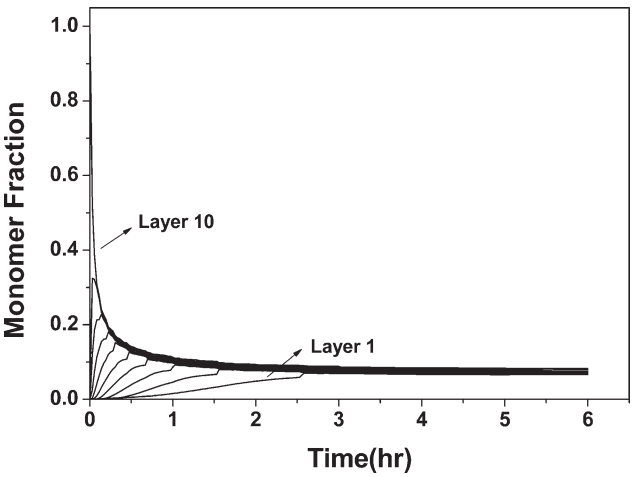

Figure 18 Monomer fraction evolution within each layer with the two-site-type MLMCM.

the monomers around the catalyst active centers are not adequate. In the reaction-dominated period, the particle grows faster than before, and the situation of monomer starvation no longer exists. At the end of polymerization, that is, the steady-state period, the layer radius no longer grows as intensively as before but remains almost unchanged. The two-site-type MLMCM, as shown in Figures 15 and 16, exhibits almost the same tendency and values during the whole polymerization.

The amount of the monomer within each layer is the outcome of diffusion accumulation (monomer diffused from the outer layer − monomer diffusing into the inner layer) on the one hand and the consumption of the monomer on the other hand. Figures 17 and 18 show the monomer fraction profiles within each layer with the single-site-type and two-site-type MLMCMs. Except for layer 10, the monomer concentrations within the layers experience a higher-to-lower process. All the monomer fractions at the end of polymerization are restrained within the range of 5–8%.

CONCLUSIONS

According to the simulation results, we can understand that the propylene polymerization process can be divided into three temporal sections: diffusion-dominated, reaction-dominated, and steady-state. In addition, the MLMCM can make better predictions of polymerization kinetics in the reaction system, and this shows that interparticle and intraparticle diffusion effects can have distinct influences on the product properties.

On the whole, simulations were performed for propylene polymerization with single-site-type and two-site-type catalysts with a novel MLMCM. Taking into consideration diffusion resistance, the MLMCM provides a precise description of the propylene polymerization process and therefore the product properties.

Certainly, this MLMCM has some limitations, such as absence of the entire polymer distribution (not presented here).[42] It is also limited for homopolymerization systems in CSTRs because of some necessary assumptions. Further improvements and development of this model are in progress in our group.

The authors thank the anonymous referees for comments on this article.

References

1. Zacca, J. J.; Debling, J. A.; Ray, W. H. Chem Eng Sci 1996, 51, 4859.
2. McKenna, T. F.; Soares, J. B. P. Chem Eng Sci 2001, 56, 3931.
3. Luo, Z. H.; Zhan, X. L.; Yang, Y. R. J Shanghai Univ 2006, 10, 274.
4. Soares, J. B. P. Chem Eng Sci 2001, 56, 4131.
5. Schmeal, W. R.; Street, J. R. AIChE J 1971, 17, 1189.
6. Galvan, R.; Tirrell, M. Comput Chem Eng 1986, 10, 77.
7. Galvan, R.; Tirrell, M. Chem Eng Sci 1986, 41, 2385.
8. Hutchinson, R. A.; Chen, C. M.; Ray, W. H. J Appl Polym Sci 1992, 44, 1389.
9. Soares, J. B. P.; Hamielec, A. E. Polymer 1996, 37, 4599.
10. Soares, J. B. P.; Hamielec, A. E. Polymer 1996, 37, 4607.
11. Sun, J. Z.; Eberstein, C.; Reichert, K. H. J Appl Polym Sci 1997, 64, 203.
12. Rincon-Rubio, L. M.; Wilen, C. E.; Lindfors, L. E. Eur Polym J 1990, 26, 171.
13. McAuley, K. B.; MacGregor, J. F.; Hamielec, A. E. AIChE J 1990, 36, 837.
14. Soares, J. B. P.; Hamielec, A. E. Polymer 1995, 36, 2257.
15. Simon, L. C.; Soares, J. B. P.; Souza, R. F. AIChE J 2000, 46, 1234.
16. Luo, Z. H.; Zheng, Y.; Cao, Z. K.; Wen, S. H. Polym Eng Sci 2007, 47, 1643.
17. Luo, Z. H.; Zheng, Y.; Cao, Z. K.; Wen, S. H. Chin J Polym Sci 2007, 25, 365.
18. Luo, Z. H.; Wang, W.; Su, P. L. J Appl Polym Sci 2008, 110, 3360.
19. Soares, J. B. P.; Hamielec, A. C. Macromol React Eng 2007, 1, 53.
20. Platkowski, K.; Reichert, K. H. Polymer 1999, 40, 1057.
21. Gillespie, D. T. J Comput Phys 1976, 22, 403.
22. He, J. P.; Zhang, H. D.; Chen, J. M.; Yang, Y. L. Macromolecules 1997, 30, 8010.
23. Mead, D. W. J Appl Polym Sci 1995, 57, 151.
24. Butte, A.; Ghielmi, A. S. G.; Morbidelli, M. Macromol Theor Simul 1999, 8, 498.
25. Iedema, P. D.; Wulkow, M.; Hoefsloot, C. J. Macromolecules 2000, 33, 7173.
26. Hutchinson, R. A. Macromol Theor Simul 2001, 10, 144.
27. Pladis, P.; Kiparissides, C. Chem Eng Sci 1998, 53, 3315.
28. Wulkow, M. Macromol Theor Simul 1996, 5, 393.
29. Cifra, P.; Bleha, T. Polymer 2007, 48, 2444.
30. Simon, L. C.; Soares, J. B. P. Ind Eng Chem Res 2005, 44, 2461.
31. Simon, L. C.; Williams, C. P.; Soares, J. B. P.; de Souza, R. F. Chem Eng Sci 2001, 56, 4181.
32. Kakugo, M.; Sedatoshi, H.; Sakai, J.; Yokoyama, M. Macromolecules 1989, 22, 3172.
33. Noristi, L.; Marchetti, E.; Baruzzi, G.; Sgarzi, P. J Polym Sci Part A: Polym Chem 1994, 32, 3047.

34. Zacca, J. J.; Debling, J. A.; Ray, W. H. Chem Eng Sci 1997, 52, 1941.
35. Floyd, S.; Choi, K. Y.; Taylor, T. W.; Ray, W. H. J Appl Polym Sci 1986, 32, 2935.
36. Floyd, S.; Choi, K. Y.; Taylor, T. W.; Ray, W. H. J Appl Polym Sci 1986, 31, 2231.
37. Kanellopoulos, V.; Gustafsson, B.; Kiparissides, C. Macromol React Eng 2007, 2, 240.
38. Di Drusco, G.; Rinaldi, R. Hydrocarbon Process 1984, 63, 113.
39. Luo, Z. H.; Zheng, Y.; Cao, Z. K.; Xu, W. Acta Petrol Sinica 2003, 22, 85.
40. Zhen, Y. Master's Thesis, Xiamen University, 2006.
41. Flory, P. J. Principles of Polymer Chemistry; Cornell University Press: Ithaca, NY, 1953; p 46.
42. Dompazis, G.; Kanellopoulos, V.; Touloupides, V.; Kiparissides, C. Chem Eng Sci 2008, 63, 4735.